Growth and mutual interference of protein seeds under reduced gravity conditions

M. Lappa[a)]
MARS (Microgravity Advanced Research and Support Center), Via Gianturco 31, 80146, Napoli, Italy

(Received 5 August 2002; accepted 15 January 2003; published 4 March 2003)

This analysis deals with new models and computational methods as well as with novel results on the relative importance of ''controlling forces'' in macromolecular crystal growth. The attention is focused in particular on microgravity fluid-dynamic aspects and on the case of the simultaneous growth of different seeds. A ''kinetic-coefficient-based'' volume of fraction method is specifically and carefully developed according to the complex properties and mechanisms of macromolecular protein crystal growth. It is shown that the size and the shape of the growing crystals play a ''critical role'' in the relative importance of surface effects and in determining the intensity of convection. Convective effects, in turn, are found to impact growth rates, macroscopic structures of precipitates, particle size and morphology as well as the mechanisms driving growth. The face growth rates in particular depend on the complex multicellular structure of the convective field and on associated ''pluming phenomena.'' The relative importance of mass transport in liquid phase and surface attachment kinetics is investigated. The simulations show that it does not behave as a ''fixed'' parameter and that different crystallization conditions may occur in the protein chamber due to mutual interference of the growing seeds, complex convective effects and the ''finite size'' of the reactor. © *2003 American Institute of Physics.* [DOI: 10.1063/1.1557916]

I. INTRODUCTION

Macromolecules are extremely complex physical–chemical systems whose properties vary as a function of many environmental influences.[1] Several studies have shown that the crystallization process is sensitive to a very large amount of parameters: e.g., temperature, supersaturation, defect formation, shear forces, etc. The problem is very complex and far to be well understood. An exhaustive review of the previous fundamental protein crystal growth and morphology experimental studies has been given in Monaco and Rosenberger[2] and Coriell, Chernov, Murray, and McFadden.[3]

With regard the rate of growth of protein crystals, it is well known that there are two important effects to consider: the transport of molecules to the face of a growing nucleus or crystal, and the frequency with which the molecules orient and attach themselves to the growing surface (i.e., crystal growth rates can be considered in terms of mass transport in liquid phase and attachment kinetics). However the results provided by the different investigators do not agree about the relative importance of these two effects. The presence of a distinct boundary layer about the crystals supports the idea of competitive transport and attachment kinetics in limiting the crystal growth rate. However, the interplay between these effects is still unknown even if the case of mass transport in liquid phase simply governed by diffusion is considered. Further complication occurs if convective transport in liquid phase is taken into account. About this topic some interesting information has been provided by recent experiments in space.

Crystallization experiments carried out in microgravity conditions, in fact, have yielded protein crystals that resulted in diffraction data of significantly higher resolution than the best crystals of these proteins grown on Earth. Since an obvious difference between the space and Earth based experiments is the magnitude of the buoyancy forces in the solution, the role of solutal convection in protein crystal growth has been proved to be very important.

Superimposed on this is the poor state of our current understanding of the effect of the mutual interference among growing seeds. It is expected that mutual interference can affect the local growth rates as well as the mechanisms driving growth. Under pure diffusive regime, the depletion zones associated to the different growing seeds may intersect and overlap leading to competition for growth; under convective conditions the behavior may be very complex.

An excellent effort to the understanding of the interaction between organic crystal growth and convection has been given by Lin, Rosenberger, Alexander, and Nadarajah.[4] In their numerical simulations the protein concentration at the crystal interface was computed using a kinetic-coefficient-based surface condition. However, they investigated the depletion zone and the growth rate of a single seed. The increase of mass (size) of the growing crystal due to protein depletion in the liquid phase was not taken into account (fixed size model). According to different experimental studies (see, e.g., Pusey, Snyder, and Naumann[5]), on the other hand, it seems that the increasing size of a growing crystal plays a ''critical role'' in the phenomena under investigation

[a)]Author to whom correspondence should be addressed. Also at: Via Salvator Rosa 53, San Giorgio a Cremano, 80046 Napoli, Italy; fax: +39-81-6042100; electronic mail: marlappa@unina.it and lappa@marscenter.it

and in particular in determining the relative importance of surface attachment kinetics and mass transport in liquid phase under diffusive or convective conditions.

From a numerical point of view, strictly speaking, the growing crystal gives rise to a moving boundary problem. Moving boundary problems are still a challenging task for computational fluid-dynamics, have instigated much research, and have led to many different solutions.[6–12]

Volume of fluid methods (VOF) and level-set methods have became popular in the last years. In particular, they have been used for the simulation of typical problems associated to gas–liquid or liquid–liquid systems where the interfacial surface tension plays a ''critical role.'' On the other hand, the ''enthalpy method'' has been successfully applied to the case of thermal phase change problems characterized by the presence of moving solid–melt interfaces associated to the heating or the cooling of the system under investigation. However, a complete numerical method aimed at the (''moving boundary'') simulation of the growth or dissolution of organic crystals by solubility modulation is still missing.

A very interesting and pioneer study related to the interplay between crystal growth and convection and to the associate moving boundary problem has been carried out recently by Noh, Koh, and Kang.[13] They investigated the growth behaviors of a single precipitate particle in a supersaturated solution under the effect of ''*a priori*'' (well-defined) imposed ''ambient'' flows. The Stokes flow approximation was assumed to simplify the model. Numerical solutions were obtained through numerically generated orthogonal curvilinear co-ordinate system, automatically adjusted to fit the boundary shape at any instant.

Aim of the present paper is (1) to introduce a novel and robust numerical method to handle the complex phenomena related to the growth or resolution of organic crystals according to the protein concentration and solubility distribution in the feeding solution, taking into account the size variation, the morphology of the crystal as well as the possibility of the simultaneous growth of different seeds; (2) to shed some light on the complex interplay and relative importance of the surface attachment kinetics and the mass transport in liquid phase; (3) to investigate the role of convection in these behaviors.

The present contribution appears as the first attempt to analyze in detail these behaviors.

II. MATHEMATICAL MODEL AND NUMERICAL METHOD

A. The OCGVOF method: General properties

This section describes the properties of the sophisticated numerical algorithm proposed here for the case of crystallization of organic substances due to solubility modulation (OCGVOF–organic crystal growth volume of fraction method). The OCGVOF method, which, similarly to VOF and enthalpy methods, is a single region formulation, allows a fixed-grid solution to be undertaken and is, therefore, able to utilize standard solution procedures for the fluid flow and species equations directly, without resorting to mathematical manipulations and transformations.

This method accounts for the solid mass stored in the generic computational cell by assigning an appropriate value of ϕ (phase field variable) to each mesh point ($\phi=1$ crystal, $\phi=0$ feeding solution and $0<\phi<1$ for an interfacial cell). The key element for the OCGVOF method is its technique for adjourning ϕ. Upon changing phase, the ϕ-value of the cell is adjusted to account for mass release or absorption, this adjustment being reflected in the protein concentration distribution as either a source or sink. The modeling of these phenomena leads to the introduction of a group of differential equations, strictly related, from a mathematical point of view, to the ''kinetic conditions'' used to model mass transfer at the crystal surface. Surface attachment kinetics at the crystal surface depend on the local value of solubility and on a coefficient λ (kinetic coefficient) whose value may be different according to the local orientation of the crystal surface (surface-orientation-dependent growth; this situation occurs for crystalline proteins which have high anisotropy, i.e., preferred orientations in either their surface energy or atomic attachment kinetics); using mass balance (see, e.g., Rosenberger[14]), and assuming a linear dependence of the growth rate by the interface supersaturation (see, e.g., Lin *et al.*[4]), one obtains

$$\left(\frac{D}{\rho_P-\rho_C C_i/\rho_S}\right)\left.\frac{\partial C}{\partial n}\right|_i=\lambda(\hat{\underline{n}})\left(\frac{C_i-S}{S}-\delta_O\right), \tag{1}$$

where C_i is the concentration of the protein at the crystal surface, D is the related diffusion coefficient, S is the solubility (its value is function of the local concentration of the precipitant agent and/or of temperature), ρ_P and ρ_C are the protein mass density and the total mass density in the crystal, ρ_S is the total density of the solution, δ_O is the width of the supersaturation range in which no growth occurs, $\lambda(\hat{\underline{n}})$ is the kinetic coefficient and $\hat{\underline{n}}$ is the unit vector perpendicular to the crystal surface pointing into the liquid. The parameter δ_O takes into account the so-called ''dead zone,'' that according to many investigators, in the case of organic substances, is due to the absorption of impurities that lead to strong retardation of the growth kinetics.

Whenever protein in solute phase and solid crystal coexist in equilibrium (saturation condition)

$$C_i=S. \tag{2}$$

In a saturated solution, two states exist in equilibrium, the solid phase, and one consisting of molecules free in solution. At saturation, no net increase in the proportion of solid phase can accrue since it would be counterbalanced by an equivalent dissolution. Thus ''crystals do not grow from a saturated solution.'' The system must be in a nonequilibrium, or supersaturated state to provide the thermodynamic driving force for crystallization (McPherson[1]).

Solution must by some means be transformed or brought into the supersaturation state whereby its return to equilibrium, forces exclusion of solute molecules into the solid state, the crystal. As long as $C_i<S$, more solid material will

dissolve if any. If, on the other hand, $C_i > S$, material will condense on any material *already existing* and augment its size (the solution is said to be *supersaturated* when the solute content is greater than S, and the degree of supersaturation σ is defined by $\sigma = C/S$). The ''growth regime'' may be very complex and nonlinear (see, e.g., Vekilov *et al.*[15]). Its features depend on several parameters and in particular it is function of the ratio between surface-attachment kinetics [modeled by Eq. (1)] and mass transport in liquid phase (diffusive or convective).

B. Governing field equations

The model is based on the mass balance equations. Therefore, in absence of convection, the diffusion of protein is governed by the equation

$$\frac{\partial C}{\partial t} = (1-\phi)\nabla^2 C. \tag{3a}$$

The diffusion of the precipitant agent is governed by the equation (it is assumed that precipitant does not precipitate in solid phase)

$$\frac{\partial C_{\text{salt}}}{\partial t} = \frac{D_{\text{salt}}}{D}(1-\phi)\nabla^2 C_{\text{salt}}. \tag{3b}$$

The nondimensional form of the equations results from scaling the lengths by a reference distance (L), the time by L^2/D; the initial value of protein and precipitant agent (salt) are $C_{(o)}$ and $C_{\text{salt}(o)}$ respectively. Note that concentrations are not posed in nondimensional form (g cm^{-3}).

In presence of convection, the flow is governed by the continuity, Navier–Stokes and species equations, that in nondimensional conservative form read

$$\underline{\nabla}\cdot\underline{V} = 0, \tag{4}$$

$$\frac{\partial \underline{V}}{\partial t} = -\underline{\nabla} p - \underline{\nabla}\cdot[\underline{V}\underline{V}] + \text{Sc}\,\nabla^2\underline{V} + \text{Sc}\,\text{Ra}\left(\frac{C}{C_{(o)}} - 1\right)\underline{i_g} + \frac{D_{\text{salt}}}{D}\text{Sc}\,\text{Ra}_{\text{salt}}\left(\frac{C_{\text{salt}}}{C_{\text{salt}(o)}} - 1\right)\underline{i_g} - \text{Sc}\frac{1}{\eta}\underline{V}, \tag{5}$$

where ν is the kinematic viscosity, $\text{Sc} = \nu/D$, $\text{Ra} = g\beta_{\text{prot}}C_{(o)}L^3/\nu D$ and $\text{Ra}_{\text{salt}} = g\beta_{\text{salt}}C_{\text{salt}(o)}L^3/\nu D_{\text{salt}}$ (the Boussinesq approximation is used to model the buoyancy forces, β_{prot} and β_{salt} are the solutal expansion coefficients related to organic substance and salt, respectively)

$$\frac{\partial C}{\partial t} = (1-\phi)[-\underline{\nabla}\cdot(\underline{V}C) + \nabla^2 C], \tag{6}$$

$$\frac{\partial C_{\text{salt}}}{\partial t} = (1-\phi)\left[-\underline{\nabla}\cdot(\underline{V}C_{\text{salt}}) + \frac{D_{\text{salt}}}{D}\nabla^2 C_{\text{salt}}\right], \tag{7}$$

where V and p are the nondimensional velocity and pressure. The reference velocity and pressure are D/L and $\rho_S D^2/L^2$ respectively. Note that in case solubility modulation is induced by temperature control, Eq. (7) must be replaced by the energy equation.

Assumptions invoked in the development of equations for this continuum model include: laminar flow, Newtonian behavior of the phases (this implies that solids should be treated as highly viscous fluids), constant phase densities (and Boussinesq approximation).

Moreover the solid phase (crystal) is assumed to be nondeforming and free of internal stress, while the multiphase region (region where phase change occurs) is viewed as a porous solid characterized by an isotropic permeability η by analogy with the enthalpy methods (see, e.g., Voller *et al.*,[9] Bennon and Incropera[10] and Brent *et al.*[11]).

The species equations (6) and (7) are solved throughout the computational domain including both the solid and liquid phases. The presence of the term $(1-\phi)$ ensures in fact that the solid phase is impermeable to protein and precipitant in solute phase.

An important problem with fixed-grid solution procedures, is accommodating the zero velocity condition, which is required as a liquid region turns to solid. Various methods can be used in principle to ''switch off'' velocities in computational cells that are becoming solid (or ''switch on'' velocities in the reverse case). Here the ''porosity approach'' is used. It requires that computational cells that are undergoing a phase change are modeled as a pseudo-porous media, with the porosity η being a function of ϕ ranging between 0 (fully liquid cell) and 1 (fully solid cell). For the present case of macromolecular organic crystal growth, this assumption is based directly on the fact that solid formation occurs as a ''permeable'' crystalline matrix which coexists with the liquid phase. The term $-\text{Sc}/\eta$ in Eq. (5) is the Darcy term added to the momentum equation to eliminate convection in the solid phase. In the present analysis permeability is assumed to vary according to the Carman–Kozeny equation (Bennon and Incropera[10] and Brent *et al.*[11])

$$\eta = \frac{(1-\phi)^3}{\phi^2}. \tag{8}$$

In the pure solid ($\phi = 1$) and pure liquid ($\phi = 0$), Eq. (8) reduces to the appropriate limits, namely $\eta = 0$ and $\eta = \infty$, respectively. In practice the effect of η is as follows: In full liquid elements $1/\eta$ is zero and has no influence; in elements that are changing phase, the value of η will dominate over the transient, convective and diffusive components of the momentum equation, thereby forcing them to imitate Carman–Kozeny law; in totally solid elements, the final large value of $1/\eta$ will swamp out all terms in the governing equations and force any velocity predictions effectively to zero.

Since the momentum equation is valid throughout the entire domain, explicit consideration need not be given to boundaries between solid, multiphase, and liquid regions.

C. Phase field equation

On the surface of the crystal ($|\underline{\nabla}\phi| \neq 0, 0 < \phi < 1$), protein concentration must satisfy the kinetic condition that in nondimensional form reads

$$\left(\frac{1}{\rho_P - \rho_C C_i/\rho_S}\right)\left.\frac{\partial C}{\partial n}\right|_i = \tilde{\lambda}(\hat{\underline{n}})(\sigma_i - 1 - \delta_O), \tag{9}$$

where $\tilde{\lambda}=\lambda L/D$, S is function of the local precipitant concentration and

$$\underline{\hat{n}}=-\frac{\underline{\nabla}\phi}{|\underline{\nabla}\phi|}=(\alpha,\beta), \tag{10}$$

$$\alpha=-\frac{\partial\phi}{\partial x}\Big/\sqrt{\left(\frac{\partial\phi}{\partial x}\right)^2+\left(\frac{\partial\phi}{\partial y}\right)^2}, \tag{11a}$$

$$\beta=-\frac{\partial\phi}{\partial y}\Big/\sqrt{\left(\frac{\partial\phi}{\partial x}\right)^2+\left(\frac{\partial\phi}{\partial y}\right)^2}, \tag{11b}$$

since $\partial C/\partial n=\alpha(\partial C/\partial x)+\beta(\partial C/\partial y)$, (hereafter the subscript i is omitted) Eq. (9) can be written as

$$\alpha\frac{\partial C}{\partial x}+\beta\frac{\partial C}{\partial y}=\tilde{\lambda}(\alpha,\beta)(\rho_P-\rho_C C/\rho_S)(C/S-1-\delta_O), \tag{12}$$

$\tilde{\lambda}(\rho_P-\rho_C C/\rho_S)(C/S-1-\delta_O)$ represents the mass exchange flux between solid and liquid phase (i.e., crystal and protein solution). The mass stored in computational cells that are undergoing phase change can be computed according to the equation

$$\frac{\partial M}{\partial t}=\frac{\lambda(\alpha,\beta)L^4}{D}(\rho_P-\rho_C C/\rho_S)(C/S-1-\delta_O)ds, \tag{13}$$

where ds is the ''reconstructed'' portion of the crystal surface (by definition perpendicular to the interface normal vector $\underline{\hat{n}}$) ''bounded'' by the frontier of the control volume (computational cell) located astride the crystal surface.

The nondimensional volume of the crystal mass stored in a grid cell can be computed as (ρ_P is the protein mass density in the crystal)

$$dv|_{\text{stored}}=\frac{1}{L^3}\frac{M}{\rho_P}, \tag{14}$$

correspondingly

$$\phi=\frac{dv|_{\text{stored}}}{dv}, \tag{15}$$

where dv is the volume of the computational cell.

Therefore, the phase field equation reads

$$\frac{\partial\phi}{\partial t}=0, \quad \text{if} \quad |\underline{\nabla}\phi|=0,$$

$$\frac{\partial\phi}{\partial t}=\frac{\tilde{\lambda}(\alpha,\beta)(\rho_P-\rho_C C/\rho_S)(C/S-1-\delta_O)ds}{\rho_P dv}, \quad \text{if} \quad |\underline{\nabla}\phi|\neq 0,\ 0<\phi<1, \tag{16}$$

with C satisfying Eq. (12).

From mass balance the solution for the normal velocity at the interface is

$$\underline{V}\cdot\underline{\hat{n}}=(\rho_C/\rho_S)\theta^*, \quad \text{if} \quad |\underline{\nabla}\phi|\neq 0,\ 0<\phi<1, \tag{17a}$$

where ρ_S (total density of the solution) is computed as $\rho_S=\rho_{H_2O}(1+\beta_{\text{prot}}C_{(o)}+\beta_{\text{salt}}C_{\text{salt}(o)})$ and the nondimensional growth rate (see, e.g., Pusey *et al.*[5]) is computed as

$$\theta^*=\left(\frac{1}{\rho_P-\rho_C C/\rho_S}\right)\frac{\partial C}{\partial n}=\tilde{\lambda}(\underline{\hat{n}})(\sigma-1-\delta_O), \tag{17b}$$

with C satisfying Eq. (12).

Equations (12), (16), and (17) behave as ''moving boundary conditions,'' their solution being strictly associated to the computational check on the value of ϕ and its gradient. Note that, typically, for organic crystal growth, the normal velocity at the interface is very small with respect to buoyancy induced velocities even if the gravity acceleration is reduced of several orders of magnitude in space, and for this reason it could be neglected.

D. Discretization

Equations (4)–(7) subjected to the initial and boundary conditions are solved numerically in primitive variables by a control volume method. The domain is discretized with a uniform mesh and the flow field variables defined over a staggered grid. Forward differences in time and upwind schemes in space (second-order accurate) are used to discretize the partial differential equations, obtaining (n superscript indicates time step)

$$\underline{V}^{n+1}=\underline{V}^n+\Delta t\Bigg[-\underline{\nabla}\cdot(\underline{V}\underline{V})+\text{Sc}\,\nabla^2\underline{V}+\text{Sc}\,\text{Ra}\left(\frac{C}{C_{(o)}}-1\right)\underline{i_g}+\frac{D_{\text{salt}}}{D}\text{Sc}\,\text{Ra}_{\text{salt}}\left(\frac{C_{\text{salt}}}{C_{\text{salt}(o)}}-1\right)\underline{i_g}\Bigg]^n-\frac{\text{Sc}}{\eta}\underline{V}^{n+1}-\Delta t\underline{\nabla}p^n, \tag{18}$$

$$C^{n+1}=C^n+\Delta t(1-\phi^n)[-\underline{\nabla}\cdot[\underline{V}C]+\nabla^2 C]^n, \tag{19}$$

$$C_{\text{salt}}^{n+1}=C_{\text{salt}}^n+\Delta t(1-\phi^n)\Bigg[-\underline{\nabla}\cdot[\underline{V}C_{\text{salt}}]+\frac{D_{\text{salt}}}{D}\nabla^2 C_{\text{salt}}\Bigg]^n. \tag{20}$$

The orientation of the surface of the crystal is used in determining the face fluxes for the computation of C at the crystal surface [Eq. (12)]. The interface orientation depends on the direction of the volume fraction gradient of the phase within the cell, and that of the neighbor cell (or cells) sharing the face in question.

The unit vector $\underline{\hat{n}}$ results from the gradient of a smoothed phase field $\tilde{\phi}$, where the transition from one phase to the other takes place continuously over several cells (4 or 5). The smoothed phase field $\tilde{\phi}$ is obtained by convolution of the unsmoothed field ϕ with an interpolation function.

Depending on the interface's orientation, concentration gradients are discretized by forward or backward schemes. For this reason Eq. (12) in discretized form reads

$$\alpha>0,\beta>0: \quad C_{i,j}^{n+1}=\frac{[\tilde{\lambda}(1+\delta_O)(\rho_P-\rho_C C_{i,j}^{n+1}/\rho_S)+\alpha C_{i+1,j}^{n+1}/\Delta x+\beta C_{i,j+1}^{n+1}/\Delta y]}{[\tilde{\lambda}(\rho_P-\rho_C C_{i,j}^{n+1}/\rho_S)/S+\alpha/\Delta x+\beta/\Delta y]}, \tag{21a}$$

$$\alpha<0,\beta>0: \quad C_{i,j}^{n+1}=\frac{[\tilde{\lambda}(1+\delta_O)(\rho_P-\rho_C C_{i,j}^{n+1}/\rho_S)-\alpha C_{i-1,j}^{n+1}/\Delta x+\beta C_{i,j+1}^{n+1}/\Delta y]}{[\tilde{\lambda}(\rho_P-\rho_C C_{i,j}^{n+1}/\rho_S)/S-\alpha/\Delta x+\beta/\Delta y]}, \tag{21b}$$

$$\alpha>0,\beta<0: \quad C_{i,j}^{n+1}=\frac{[\tilde{\lambda}(1+\delta_O)(\rho_P-\rho_C C_{i,j}^{n+1}/\rho_S)+\alpha C_{i+1,j}^{n+1}/\Delta x-\beta C_{i,j-1}^{n+1}/\Delta y]}{[\tilde{\lambda}(\rho_P-\rho_C C_{i,j}^{n+1}/\rho_S)/S+\alpha/\Delta x-\beta/\Delta y]}, \tag{21c}$$

$$\alpha<0,\beta<0: \quad C_{i,j}^{n+1}=\frac{[\tilde{\lambda}(1+\delta_O)(\rho_P-\rho_C C_{i,j}^{n+1}/\rho_S)-\alpha C_{i-1,j}^{n+1}/\Delta x-\beta C_{i,j-1}^{n+1}/\Delta y]}{[\tilde{\lambda}(\rho_P-\rho_C C_{i,j}^{n+1}/\rho_S)/S-\alpha/\Delta x-\beta/\Delta y]}, \tag{21d}$$

$C_{i,j}^{n+1}$ is computed from Eq. (21) iterating up to reach convergence, then the phase variable is updated using Eq. (16)

$$\phi_{i,j}^{n+1}=\phi_{i,j}^{n}+\Delta t\frac{\tilde{\lambda}(\rho_P-\rho_C C_{i,j}^{n+1}/\rho_S)(C_{i,j}^{n+1}/S-1-\delta_O)\Delta s}{\rho_P \Delta x \Delta y}. \tag{22}$$

According to Eqs. (21) and (22), if the protein concentration is locally depleted, correspondingly, the solid mass stored in the computational cell grows and the phase variable is increased; on the other hand if mass stored in the cell begins to redissolve, protein is released in solute phase and the local value of protein concentration is increased. These phenomena are driven by the attachment kinetic condition, i.e., the existing deposit grows if protein concentration is larger than S and the mass exchange is proportional to the local value of the orientation-dependent kinetic coefficient; in the opposite situation, i.e., in case protein concentration becomes smaller than S, deposit begins to redissolve. The solubility is function of the precipitant agent (salt) concentration and for this reason the phenomena are mainly governed by the distribution of this agent [i.e., by Eq. (20), or by temperature in case solubility modulation is induced by thermal control].

Note that the present model is two dimensional. Two-dimensional computations do not allow to capture morphological and/or fluid-dynamic instabilities dealing with the third dimension (z). Note that the numerical simulations of these aspects would require ''massively'' parallel supercalculus. However two-dimensional simulations can provide useful information about the dynamics of the phenomena under investigation if the dimension of the reactor along z is of the same order of the size of the crystals and if the residual-g leading to the onset of convection does not have components in the z direction.

In Eq. (22) Δs is the ''reconstructed'' portion of the solid wall. The determination of Δs requires a well defined ''interface-reconstruction'' technique (the shape of the crystal for a fixed time is not known a priori and must be determined as part of the solution, see, e.g., the nonconnecting straight lines technique of Gueyffier *et al.*[8]).

The implementation of the MAC method for the solution of Eq. (18) is not described here for the sake of brevity (for further details see, e.g., Monti *et al.*[16]). Parallel supercalculus is used due to the enormous time required for the computations (although the model is two dimensional). The problem is split in two problems, one parabolic and the other elliptic. A parallel algorithm, explicit in time, is utilized to solve the parabolic equations (momentum and species equations). A parallel multisplitting kernel is introduced for the solution of the pseudo-pressure elliptic equation, representing the most time-consuming part of the algorithm. A grid-partition strategy is used in the parallel implementations of both the parabolic equations and the multisplitting elliptic kernel. A message passing interface (MPI) is coded for interprocessor communications. For further details see, e.g., Lappa[17] and Lappa and Savino.[18] The code has been validated through comparison with the numerical results of Lin *et al.*[4] The results show good agreement. The maximum velocity and the corner growth rate at $t=18\,000$ s are 8.1×10^{-4} cm s^{-1} and 41 Å s^{-1} in good agreement with the values obtained by Lin *et al.*[4] (8.6×10^{-4} cm s^{-1} and 44 Å s^{-1}, respectively). The small difference between the present results and those obtained by Lin *et al.*[4] could be explained according to the fact that during the five hours simulations the crystal undergoes small dimensional changes that were not taken into account in their model.

III. RESULTS

Hen egg white lysozyme is used as model protein, being a well-characterized molecule ($Sc=8.6\times10^3$, see Table I for the properties and Otàlora and Garcìa-Ruiz[19] for the dependence of the solubility on salt concentration). The precipitant agent is NaCl.

TABLE I. Properties and operating conditions.

D_{lys} [cm^2 s^{-1}]	10^{-6}
D_{NaCl} [cm^2 s^{-1}]	10^{-5}
ν [cm^2 s^{-1}]	8.63×10^{-3}
ρ_C [g cm^{-3}]	1.2
β_{lys} [g^{-1} cm^3]	0.3
β_{NaCl} [g^{-1} cm^3]	0.6
ρ_P [mg ml^{-1}]	820
λ [Å s^{-1}]	$\cong10$
δ_o [−]	2
T [°C]	18
pH	4.5

TABLE II. Grid refinement study (maximum growth rate and maximum velocity as function of the number of grid points at $t=4.0\times10^5$ s, vertical configuration).

Grid	θ_{max} [Å/s]	$V_{max}\times10^5$ [cm/s]
100×33	7.938	1.965
150×50	9.241	2.124
200×75	10.032	2.203
300×100	10.833	2.352
400×130	10.984	2.382

Crystal growth from supersaturated solutions proceeds by the incorporation of growth units (atoms, molecules or small aggregates) from the solution to the crystal surface. This incorporation produces a concentration depletion zone around the crystals. The size and shape of the depletion zone are controlled by the coupled transport of the crystallizing species in solution to the growing surface and the processes allowing these species to be incorporated into the lattice. In order to characterize these behaviors a nondimensional parameter (γ) is introduced.

If attachment kinetics is the rate-limiting step in the growth process, $C_i=C_B$ (C_B bulk protein concentration) and the local supersaturation will be approximately the bulk supersaturation. On the other hand, if the growth rate is limited by transport (convective or diffusive) of solute to the growth interface, $C_i=S$. These processes can be characterized (Pusey *et al.*[5]) by use of the surface coefficient γ defined as

$$\gamma=\frac{(C_B-C_i)}{(C_B-S)}, \tag{23}$$

this coefficient is a measure of the relative importance of surface kinetics versus transport as the rate-limiting step in the growth of crystals. For growth controlled by surface kinetics $C_i\rightarrow C_B$ and $\gamma\rightarrow0$; for a transport controlled process, $C_i\cong S$ and $\gamma\rightarrow1$.

Transport and surface kinetics processes can be considered competitive for $\gamma\cong0.3$–0.5.

In order to discern the effect of convection with respect to other effects, the simulations are carried out under pure diffusive transport regime and in presence of buoyancy forces.

Table II shows a grid refinement study carried out to ensure good resolution and grid-independence of the results discussed in Secs. III A and III B (grid-independence is achieved for a mesh of 300×100 points).

A. Growth and mutual interference under diffusive transport regime

In the present paragraph, the growth of two seeds of lysozyme under diffusive transport conditions is simulated. For the sake of simplicity (aim of the present paper is merely to show the capabilities of the numerical method and how it can ''capture'' heretofore poorly understood physics and mechanics of the problem under investigation) the initial shape of the seeds is supposed to be quadrate and the kinetic coefficient is supposed to be the same for the different sides of the crystal (however the numerical method can handle complex shapes and anisotropic growth as shown in Sec. II A).

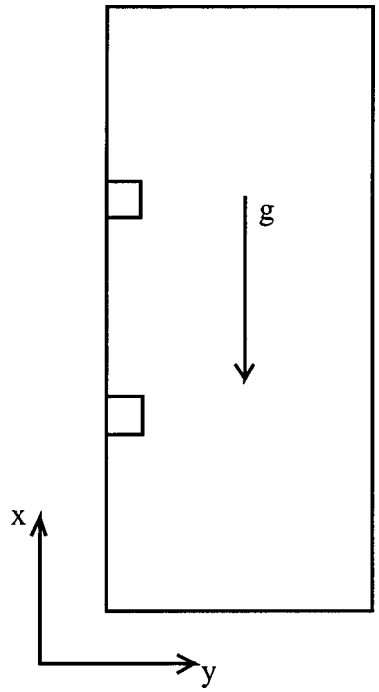

FIG. 1. Sketch of the growth reactor and of the relative position of protein seeds (isothermal protein crystal growth system: crystals of initial dimensions 1 mm × 1 mm fixed to the left wall of a 3 cm high and 1 cm wide growth cell at $x=1/3$ and $x=2/3$, respectively; $C_{lys(o)}=6\times10^{-2}$ g cm^{-3} and $C_{NaCl(o)}=2.5\times10^{-2}$ g cm^{-3}).

The crystals (1 mm × 1 mm initial size) are supposed to be fixed (e.g., by glue) to the points $x=1/3$ and $x=2/3$ of the left wall of the reactor (10 mm high and 30 mm wide test cell) used for the growth process (see Fig. 1). Growth is obtained from a supersaturated solution with $C_{lys(o)}=6\times10^{-2}$ g cm^{-3} and $C_{NaCl(o)}=2.5\times10^{-2}$ g cm^{-3} ($\sigma_{(o)}\cong6$). The frontier of the domain is supposed to be impermeable to protein and salt (therefore the salt concentration is constant). According to the grid refinement study a mesh 300×100 is used.

As seeds grow from the solution, each crystal depletes the concentration of the growth units that are incorporated into the crystal lattice producing a concentration-depleted zone around it. In this region, the solute concentration changes continuously from the concentration at the crystal face to the concentration in the bulk of the solution. The concentration profile in the concentration-depleted zone varies with time as the crystal grows and is controlled by the balance between the flow of growth units towards the crystal face and the rate of incorporation of these growth units into the crystal lattice. The kinetics of incorporation at the crystal surface are linked to the bond configuration of the crystallographic structure as discussed in Sec. II A (for the present case of isotropic growth, the kinetics of incorporation are simply linked to the value of the kinetic coefficient and to the supersaturation level), while the flow towards the crystal face is highly dependent on the symmetry or deformation of the concentration pattern, which turn out to be crucial for the overall crystal-growth process.

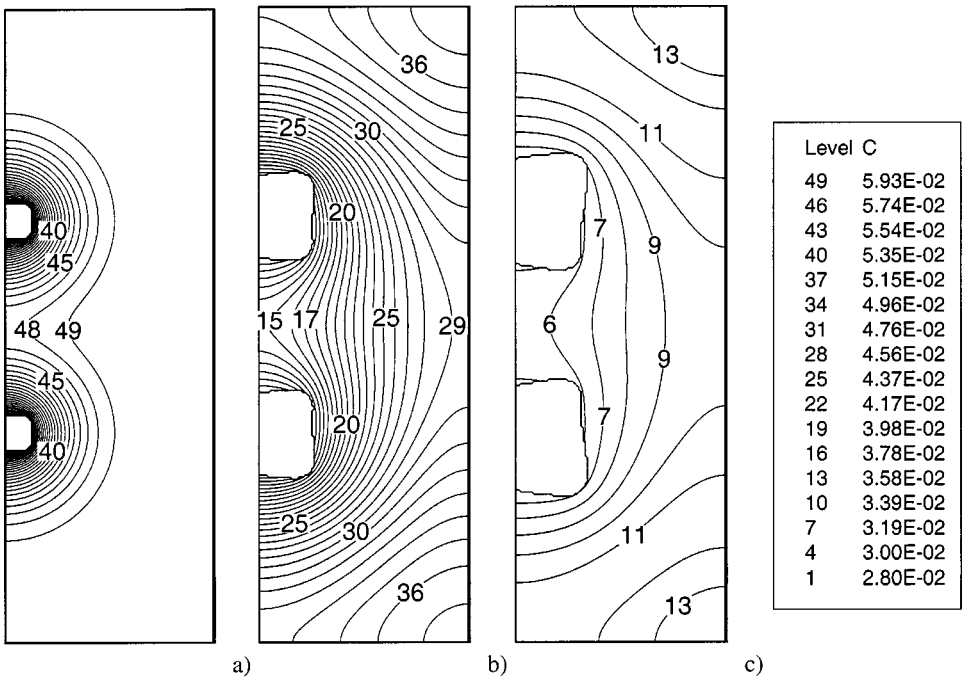

FIG. 2. Snapshots of growing crystals and concentration distribution under diffusive transport regime: (a) $t=3.6\times10^4$ s, (b) $t=5.4\times10^5$ s, (c) $t=1.33\times10^6$ s.

Regarding this aspect, note that after an initial transient behavior, the depletion zones for the two growing seeds intersect and overlap (Fig. 2). At this stage the growth dynamics of the two crystals cannot be considered independent and mutual interference occurs. Both the crystals, in fact, absorb protein from the intermediate region [Figs. 2(b) and 2(c)]. This leads to competition for growth and to a lower value of the protein concentration there. A mirror symmetric behavior occurs, however, with respect to $x=1/2$ due to the intrinsic symmetry of the system and absence of convection.

According to the ''double depletion'' and consequent limited availability of protein in the intermediate zone, the crystals exhibit lower growth rates for the sides facing this region (Fig. 3).

A further level of complication arises if the phenomena are described in detail from a ''local'' point of view: The simulations show that corners and edges of the crystal are more readily supplied with solute than the center of sides (this leads to morphological instability and to a macroscopic depression around the center of the faces, see Fig. 4). This is due to the diffusive pattern of the protein concentration field around each crystal. As previously discussed, incorporation of the solute into the crystal causes a local depletion in concentration and a solutal concentration gradient to form between the bulk solution and the growth interface. The ''steepness'' of the gradient determines the rate of solute transport to the growth interface, the steepness being maximum around the corners. Superimposed on this is the fact that a protuberance on the interface sees a higher supersaturation and grows faster than a depression, which sees a lower supersaturation. Note that the onset of morphological instabilities and the existence of ''depressions'' around the center of the faces of growing crystals (shown by the present numerical results) has been often observed experimentally (Monaco and Rosenberger[2]). Figure 4 shows that the ''depth'' of the face depressions (and therefore, the difference in gradient steepness between face corner and face center) is proportional to the size of the crystals.

As time passes, the face growth rates drop with increasing face size (correspondingly, in Fig. 5 the size of the crystal tends to an asymptotic constant value). This behavior can be explained according to two effects: (a) The finite volume of the test cell (the amount of solute protein available for the growth of the solid phase is finite and decreases as time passes); (b) as the size of the face increases, more solute should be added to maintain a given face growth rate.

The growth curve has been fitted to power law (the exponent is 0.365). The deviation from diffusion-controlled growth, which would show a square-root dependence of the crystal size on time, illustrates the fact that even when diffusive transport is ensured, no guarantee exists that the crystal will grow in the diffusion-controlled regime.

Since $\gamma\cong0.3-0.5$ (Fig. 6), surface attachment kinetics and mass transport in liquid phase can be considered competitive in limiting the growth rate for both the growing crystals. After a short initial transient, however, γ decreases (Fig. 6). This is due to diffusive transport that decreases in intensity the concentration gradient between the crystals and regions far from their surface; in ''finite size'' systems the relative importance of mass transport in liquid phase with respect to surface attachment kinetics decreases as time passes due to the decrease of available protein and related gradients. This effect, of course, is enhanced if the simultaneous presence of different growing seeds is considered.

Therefore, according to the present results the growth regime depends at least on two factors: surface attachment kinetics and competition for growth that occurs when several seeds share the same reactor.

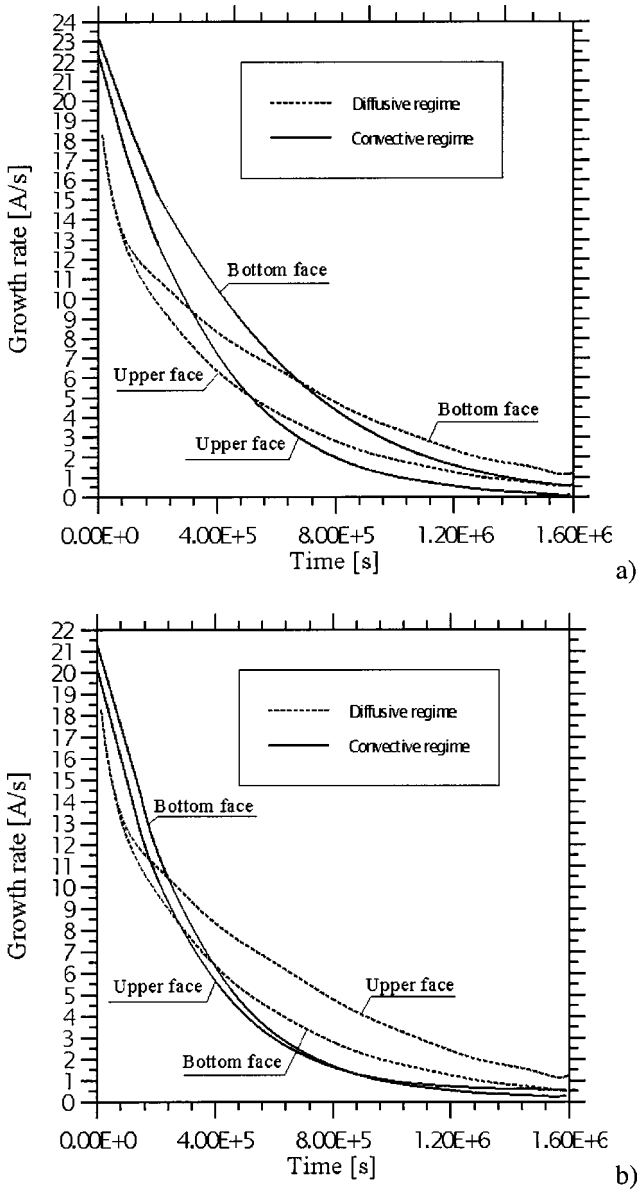

FIG. 3. Face growth rates versus time: (a) Lower crystal; (b) upper crystal.

B. Growth and mutual interference under microgravity conditions

Crystals of biological macromolecules are obtained by precipitation from supersaturated solutions and for this reason crystallization can be influenced by gravity. Concentration (density) gradients exist in the crystallizing solutions (as an intrinsic consequence of the crystal-growth process). The growth process, in fact, depletes of protein the liquid surrounding the growing crystal; the related concentration gradient implies a density gradient that, in presence of gravity, induces buoyancy driven convective flow. These phenomena occur also during experiments in space. In fact, the residual gravity estimated on board the space-shuttle and the International Space Station (ISS) is not zero, but typically of the order of 10^{-5} of earth gravity. Therefore these effects have to be evaluated under microgravity conditions, in order to properly prepare and interpret the results of crystal growth experiments in space.

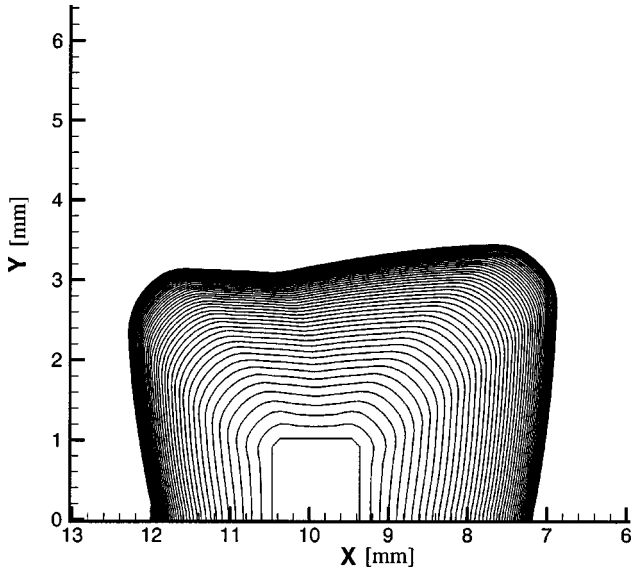

FIG. 4. Growth habit analysis: Diffusive regime, snapshots of the crystal shape versus time (lower crystal, $\Delta t = 3.6 \times 10^4$ s).

If the presence of convection ($g = 10^{-4}$ $go \rightarrow \mathrm{Ra} = 5.5 \times 10^6$) is taken into account for the same experiment investigated in Sec. III A, a flow field is driven by the density gradient around the growing crystals. Since isothermal conditions are assumed throughout the growth process, only compositional nonuniformities, that evolve in the solution due to the crystallization process, act as source for buoyancy-driven convection.

Note that two different cases are considered: Residual-g parallel to the x axis (vertical configuration) and parallel to the y axis (horizontal configuration). Both situations give insight into the effect of steady residual accelerations on the phenomena under investigation.

First the attention is focused on the vertical configuration, then the horizontal condition is discussed and compared with the vertical one.

Figure 7 show the results for the first case (vertical configuration). The flow field modifies the protein distribution around the seeds leading to a nonsymmetrical concentration pattern. The mirror symmetry with respect to the midplane $x = 1/2$ is broken. For each crystal, one recognizes the well-known convective flow pattern for solution growth with a rising ''plume'' above the seed.

The structure of the convective field is very complex. As time passes, the vortex shrinks. The contraction is strictly related to the behavior of the crystals that puff out due to growth.

Note that the rising plume created by the lower seed laps against the bottom side of the upper seed [Figs. 7(a) and 7(b)]. This phenomenon turns out to be crucial for the overall crystal-growth process. In fact the plume induces a uniformly impoverished region close to the surface of the upper crystal. For this reason the protein concentration gradients causing its growth are weakened and correspondingly the growth rate is reduced.

In order to understand the effect of convection on the system, however, it is necessary to distinguish the detailed

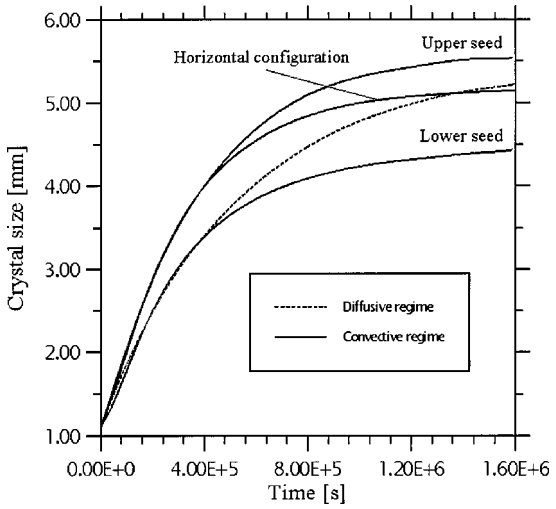

FIG. 5. Average size (along x) of the growing seeds versus time (under diffusive and convective transport regime).

description of the lower crystal behavior from the upper one.

Figure 7 show that the increase of volume of the lower crystal is more pronounced for the bottom side than for the top side. Figure 3(a) shows in detail how the convection effect results in a higher local growth rate near the surface where the flow is incoming and in a lower local growth rate near the surface where the flow is outgoing. This behavior can be explained according to two different effects.

Due to the convective structure of the flow pattern, in fact, liquid is transported towards the lower face of the crystal and in opposite direction around the upper face. According to this behavior, liquid regions (bulk) where the amount of protein available in liquid phase is still large are transported towards the bottom side of the crystal. This increases the growth rate there (a large amount of protein in solute phase is available for crystal growth). On the other hand, due to the outgoing flow, the depletion zone close to the upper face is distorted and elongated towards the top of the test cell

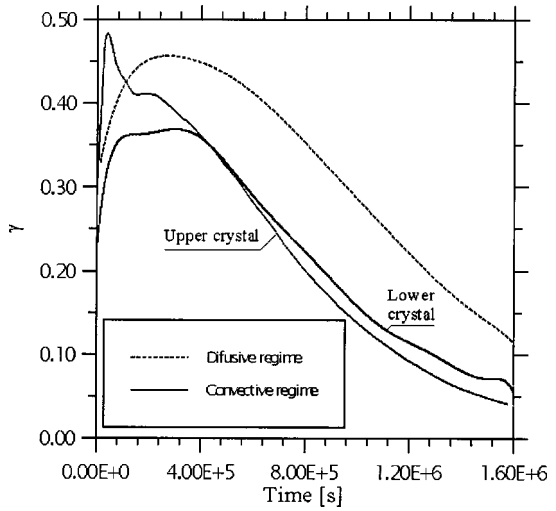

FIG. 6. Plot of γ versus time (nondimensional parameter taking into account the relative importance of surface attachment kinetics and mass transport in liquid phase).

(''plume''). This leads to a decrease of the concentration gradient (the depletion layer becomes thinner with respect to the bottom side of the crystal) and hence to a decrease of the mass exchange flux between solid and liquid phase. This explains the occurrence of a higher value of the growth rate on the bottom face of the lower crystal.

For the upper crystal the increase of size and the face growth rates do not show significant difference for the top and bottom sides [Figs. 3(b) and 7]. This occurs since in this case the incoming flow (rising plume of the lower seed) carries already impoverished liquid. The crystal is bounded by its own plume by one side and by the plume of the lower crystal by the other side. The available protein in liquid phase is small regardless the flow is incoming or outgoing. This, on the other hand, explains why the size of the lower crystal tends to be larger than that of the upper one (Figs. 5 and 7) and why face depressions do not occur for the latter. The upper seed, in fact, is embedded in a largely depleted liquid zone where the protein concentration is almost constant and the gradients are weakened; this prevents the onset of morphological instabilities.

Note that since transport of protein in liquid phase is dominated by convection, protein diffusion in the streamwise direction can be considered negligible. Thus there is no propagation of information in the upstream direction. Hence the lower crystal is not influenced directly by the upper crystal. Influence by the upper seed merely occurs via the return flow and via the total decrease of protein in liquid phase due to the simultaneous growth of two seeds in the same reactor.

Figure 3 shows that, during the first part of the growth process, the face growth rates of both the crystals under the effect of convection are considerably higher than under diffusive conditions. The growth rates decrease with increasing growth time and crystal size (the decrease being more rapid in the diffusion-dominated case). This is due to the effects already pointed out for the case of absence of convection.

The growth rate under the effect of convection is located above the corresponding one obtained under diffusive regime since convection enhances mass transport in the bulk thus increasing the rate of incorporation of the solute into the seeds.

Further to these effects one must keep in mind that there is an effect related to the fact that the magnitude of the flow is directly proportional to the size of the face upon which it is being generated. Thus, as crystals grow, solutal gradient driven flows can become a major factor for the growth rates.

As time passes, however, an inversion occurs in the behavior described above (Fig. 3). The growth rates under diffusive regime become higher than the convective ones. This behavior is strictly related to the ''finite'' amount of protein available for the crystal growth (i.e., the ''finite'' reactor size). At the beginning the convective growth rate is located above the diffusive one since solute protein is transported towards the crystal surface more rapidly with respect to a pure diffusive situation (convective motion causes fluxes in the bulk of the solution that exceed the mere diffusive ones). Due to this effect, however, the effect of the finite cell size is enhanced.

In the case of reactors having an infinite size, the con-

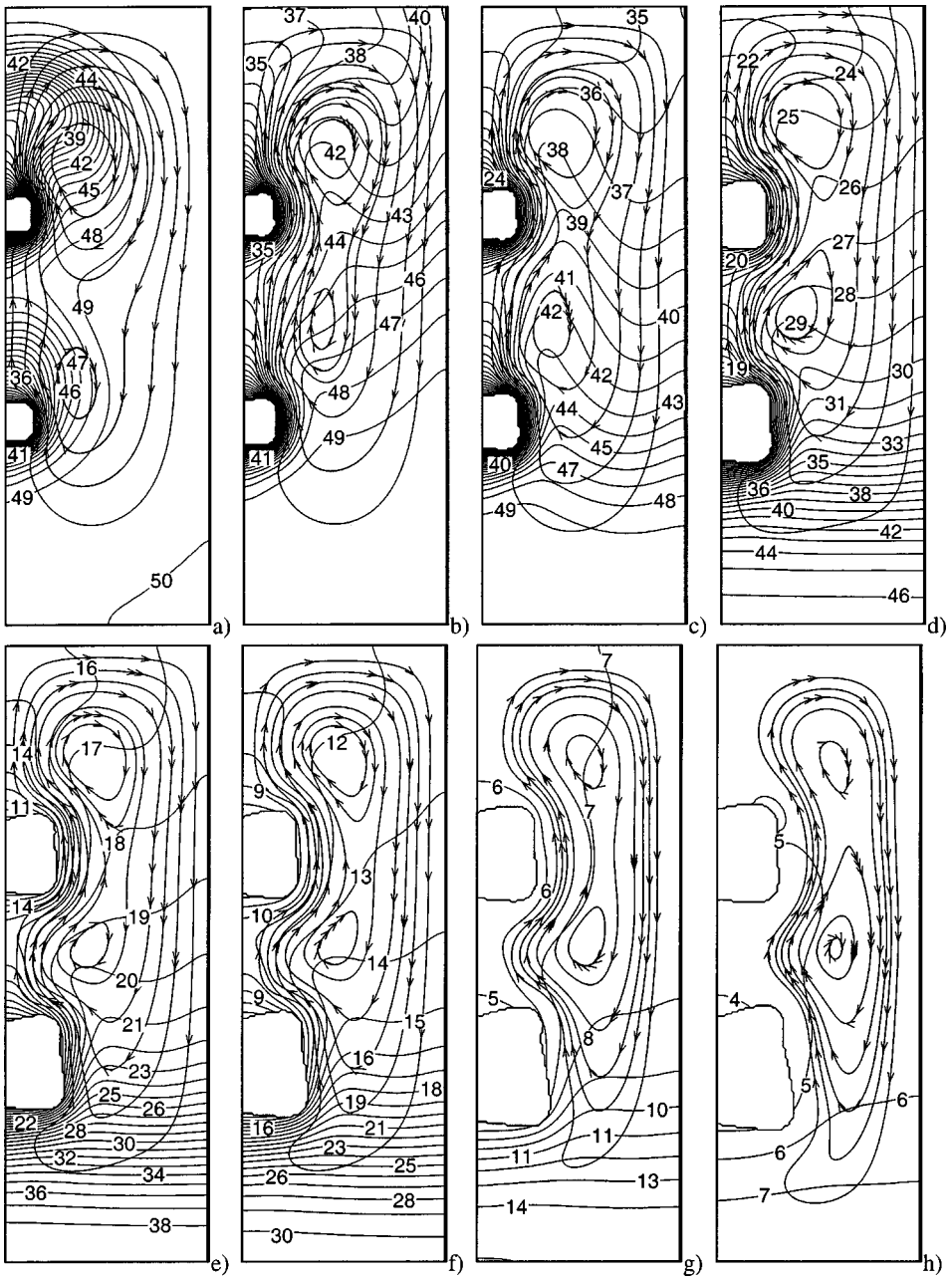

FIG. 7. Snapshots of growing crystals, concentration distribution and velocity field under microgravity conditions ($g=10^{-4}$ *go*): (a) $t=4.8\times10^4$ s, (b) $t=9.6\times10^4$ s, (c) $t=1.44\times10^5$ s, (d) $t=3.04\times10^5$ s, (e) $t=4.64\times10^5$ s, (f) $t=6.24\times10^5$ s, (g) $t=1.0\times10^6$ s, (h) $t=1.5\times10^6$ s (level $1\rightarrow2.8\times10^{-2}$ g cm^{-3}, level $50\rightarrow6\times10^{-2}$ g cm^{-3}, $\Delta c=6.4\times10^{-4}$ g cm^{-3}).

vective growth rates would be always located above the diffusive ones during the crystal growth process. However, if the initial amount of protein available for the growth is finite, this does not happen. This explains why after an initial transient time the diffusive growth rate becomes higher than the convective one and at the same time could explain some contradictory results in literature. Otàlora *et al.*[20] found a decrease of the growth rates under the effect of convection; this result is in contrast with the generalized idea that convection enhances mass transport in liquid phase increasing the growth rate. According to the present results, this counterintuitive behavior could be explained by the finite size of their reactor. Figure 6 clearly shows (as expected) that the parameter γ for the case of convection is located below the corresponding one obtained in the case of diffusive conditions; in fact convection reduces the time required to transport available protein from far regions towards the crystal surface and this decreases the relative importance of mass transport with respect to surface attachment kinetics in limiting the growth rate. Note that the time-evolution of γ under convective effects exhibits a different behavior for each seed according to its own different growth history. The role of incorporation kinetics in limiting the growth rate tends to be more important for the lower seed during the first part of the growth process and for the upper seed later.

This clearly demonstrates that, in the case of simultaneous growth of different seeds, the relative importance of mass transport in liquid phase and attachment kinetics does not behave as a ''fixed'' parameter and that different crystallization conditions may occur in a same reactor during the crystallization process due to mutual interference and complex convective effects.

Figure 8 show the results obtained in the case of horizontal configuration. As for the vertical condition, at the be-

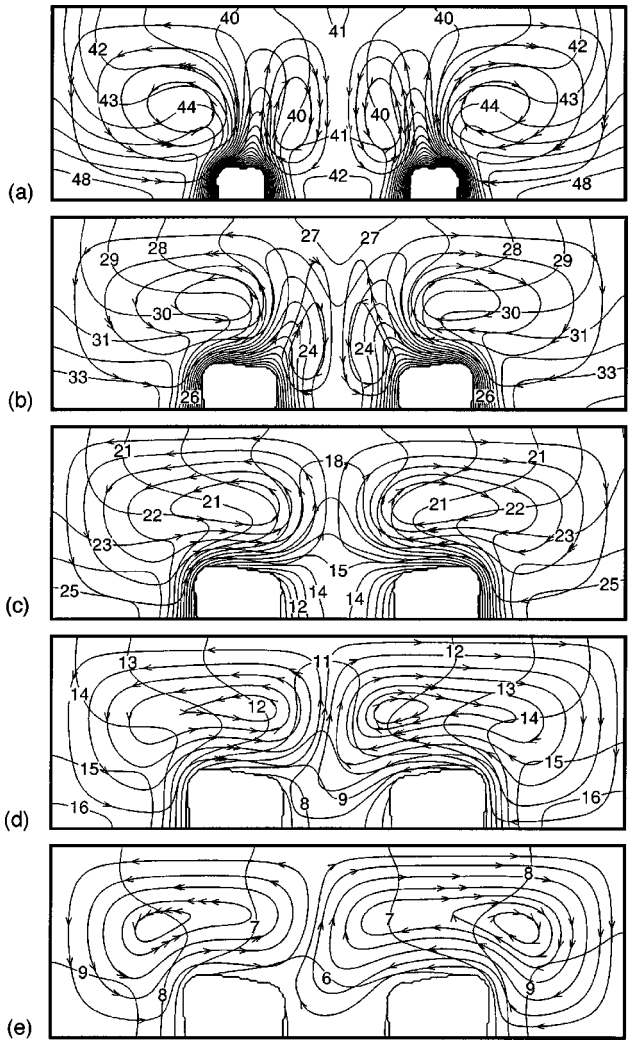

FIG. 8. Snapshots of growing crystals, concentration distribution and velocity field under microgravity conditions ($g=10^{-4}$ *go*, horizontal configuration): (a) $t=1.28\times10^5$ s, (b) $t=3.2\times10^5$ s, (c) $t=4.64\times10^5$ s, (d) $t=6.88\times10^5$ s, (e) $t=9.92\times10^5$ s (level $1\rightarrow2.8\times10^{-2}$ g cm^{-3}, level 50 $\rightarrow6\times10^{-2}$ g cm^{-3}, $\Delta c=6.4\times10^{-4}$ g cm^{-3}).

ginning one recognizes the well-known convective flow pattern with a rising plume above the seeds. Because of the geometrical constraints the rising liquid has to turn to flow along the side walls. The resulting two main vortices have symmetric form but rotate in the opposite direction, i.e., the flow is symmetric by reflection about the midplane $x=1/2$.

After 4.6×10^5 s [see Fig. 8(c)], the solutal plumes in the left and right halves of the reactor merge giving rise to a single plume located at $x=1/2$. For a further increase of the time, the simulations show that, further to morphological instabilities of the crystals (due to nonuniform transport of nutrients in the feeding solution) a true fluid-dynamic instability of the convective field appears. This instability leads to nonsymmetric patterns with respect to the midplane. It is steady in nature (stationary bifurcation) since the dynamic process of symmetry breaking is not associated with any oscillatory behavior. Prior to the onset of the bifurcation, the two vortices are one the mirror image of the other. After the transition, the flow is no longer symmetric by reflection with respect to $x=L/2$ though the geometrical configuration and the applied external forces are symmetric [Figs. 8(d) and 8(e)]. This behavior shows the "high sensitivity" of the growth process (and associated fluid-mechanics) to small asymmetries of the boundary conditions and/or to the onset of fluid-dynamic instabilities. These very interesting aspects would require further investigation and could be at the base of forthcoming analyses.

Figure 5 shows that the size of the crystals in the case of horizontal configuration lies (as expected) between the size of the upper and lower crystals yielded for the case of vertical configuration.

IV. CONCLUSIONS

A novel volume of fraction method specifically designed for the case of macromolecular (protein) growth has been introduced. This method, that eliminates the need for separate equations in each phase, by establishing conservation equations which are universally valid, allows a fixed-grid solution to be undertaken and is therefore able to utilize standard solution procedures for the fluid flow and species equations directly, without resorting to mathematical manipulations and transformations (this feature, on the other hand, facilitates a parallel implementation of the code based on a grid partition strategy).

In the OCGVOF method, the "phase field" ϕ is computed using incorporation kinetics at the surface of the crystal. These conditions are coupled to the exchange mass flux at the interface and lead to the introduction of a group of differential equations for the protein concentration at the crystal surface and the evolution of the solid mass displacement. The growth velocity is not directly imposed but it results from internal conditions related to solute transport.

The case of simultaneous growth of two protein seeds has been investigated.

The analysis of the distribution of the local growth rate along the sides of the crystals has been carried out. The face growth rates have been found to depend on the complex multicellular structure of the convective field and to be nonuniform across the crystal face (growth rate always lower at the center than at the corner). The effect of convection on the macroscopic growth rate has been proved to be nontrivial. It is strictly coupled to the interplay between crystal growth and associated "pluming phenomena" and to the "finite" size of the reactor. Under residual gravity and for the case of vertical configuration, the crystals interact mainly via the influence of the solutal plume of the lower seed on the upper seed. The rising fluid coming from the lower crystal wraps around the upper crystal and has a major role in determining the concentration distribution on its surface. The protein concentration gradients are weakened and for this reason the upper seed exhibits low values of the growth rate and the onset of morphological instabilities is prevented for this seed.

In the case of horizontal configuration the crystals interact via the competition for growth in the intermediate region. Moreover a very interesting behavior arises. The convective field can undergo a transition to a nonsymmetric flow pat-

tern. Typical flow configuration obtained prior to the onset of the instability consists of two separate mirror vortices in the left and right half of the reactor with opposite senses of rotation. The bifurcation causes an asymmetry in the structure of the two rolls.

From a global point of view, for both cases (vertical and horizontal configurations) convection enhances mass transport in liquid phase thus increasing the rate of incorporation (growth rate) of the solute into the crystal, but at the same time, it can lead to a more rapid decrease of the finite amount of protein available in solute phase and thus to a decrease of the macroscopic growth rate. The role of the changes in the size of the crystallization seeds in determining the intensity of the convective field (the magnitude of the flow, in fact, is directly proportional to the size of the face upon which it is being generated) and its structure (the increasing size of the crystals leads to a confinement of the convective field) has been pointed out.

For the first time the relative importance of surface attachment kinetics and mass transport in liquid phase has been discussed through the computation of the ''quantitative'' parameter γ. This parameter is decreased by the effect of convection and its time-evolution exhibits a different behavior for each seed according to its own different growth history. This clearly demonstrates that, in the case of simultaneous growth of different seeds, the relative importance of mass transport in liquid phase and attachment kinetics does not behave as a ''fixed'' parameter and that different crystallization conditions may occur in a same reactor due to mutual interference and complex convective effects.

A powerful mathematical tool (OCGVOF) and some information heretofore poorly understood by organic crystals growers have been made available for the scientific community to help the investigators to discern the interrelations among the various parameters under one's control (that are not independent of one another) and to elaborate rational guidelines relating to physical factors that can increase the probability of success in crystallizing protein substances. Further investigation is needed for parametric analyses of the effects described above, for more detailed investigation of the morphological (crystal) and fluid-dynamic (convective field) instabilities (and possible coupling and mutual interaction among them) and for extension to three-dimensional configurations (in this case massively parallel supercalculus would be necessary).

ACKNOWLEDGMENTS

This work has been supported by ASI (Italian Space Agency) and ESA (European Space Agency). The author would like to thank Dr. L. Carotenuto (MARS) and Professor A. A. Chernov (Universities Space Research Association—USRA) for some helpful discussions and the referees for the very constructive comments.

[1] A. McPherson, ''Current approaches to macromolecular crystallization,'' Eur. J. Biochem. **189**, 1 (1990).
[2] A. Monaco and F. Rosenberger, ''Growth and etching kinetics of tetragonal lysozyme,'' J. Cryst. Growth **129**, 465 (1993).
[3] S. R. Coriell, A. A. Chernov, B. T. Murray, and G. B. McFadden, ''Step bunching: Generalized kinetics,'' J. Cryst. Growth **183**, 669 (1998).
[4] H. Lin, F. Rosenberger, J. I. D. Alexander, and A. Nadarajah, ''Convective-diffusive transport in protein crystal growth,'' J. Cryst. Growth **151**, 153 (1995).
[5] M. L. Pusey, R. S. Snyder, and R. Naumann, ''Protein crystal growth: Growth kinetics for tetragonal lysozyme crystals,'' J. Biol. Chem. **261**, 6524 (1986).
[6] C. W. Hirt and B. D. Nichols, ''Volume of fluid (VOF) method for the dynamics of free boundaries,'' J. Comput. Phys. **39**, 201 (1981).
[7] S. Osher and J. A. Sethian, ''Fronts propagating with curvature-dependent speed: Algorithms based on Hamilton–Jacobi formulations,'' J. Comput. Phys. **79**, 12 (1988).
[8] D. Gueyffier, J. Li, A. Nadim, S. Scardovelli, and S. Zaleski, ''Volume of fluid interface tracking with smoothed surface stress methods for three-dimensional flows,'' J. Comput. Phys. **152**, 423 (1999).
[9] V. R. Voller and C. Prakash, ''A fixed grid numerical modeling methodology for convection-diffusion mushy region phase-change problems,'' Int. J. Heat Mass Transf. **30**, 1709 (1987).
[10] W. D. Bennon and F. P. Incropera, ''A continuum model for momentum, heat and species transport in binary solid–liquid phase change systems—I. Model formulation,'' Int. J. Heat Mass Transf. **30**, 2161 (1987).
[11] A. D. Brent, V. R. Voller, and J. Reid, ''Enthalpy-porosity technique for modeling convection-diffusion phase change: Application to the melting of a pure metal,'' Numer. Heat Transfer **13**, 297 (1988).
[12] M. Lappa and R. Savino, ''3D analysis of crystal/melt interface shape and Marangoni flow instability in solidifying liquid bridges,'' J. Comput. Phys. **181**, 1 (2002).
[13] D. S. Noh, Y. Koh, and I. S. Kang, ''Numerical solutions for shape evolution of a particle growing in axisymmetric flows of supersaturated solution,'' J. Cryst. Growth **183**, 427 (1998).
[14] F. Rosenberger, ''Inorganic and protein crystal growth: Similarities and differences,'' J. Cryst. Growth **76**, 618 (1986).
[15] P. G. Vekilov, J. Iwan, D. Alexander, and F. Rosenberger, ''Nonlinear response of layer growth dynamics in the mixed kinetics-bulk transport regime,'' Phys. Rev. E **54**, 6650 (1996).
[16] R. Monti, R. Savino, M. Lappa, and S. Tempesta, ''Behavior of drops in contact with pool surfaces of different liquids,'' Phys. Fluids **10**, 2786 (1998).
[17] M. Lappa, ''Strategies for parallelizing the three-dimensional Navier–Stokes equations on the Cray T3E,'' Science and Supercomputing at CINECA **11**, 326 (1997).
[18] M. Lappa and R. Savino, ''Parallel solution of three-dimensional Marangoni flow in liquid bridges,'' Int. J. Numer. Methods Fluids **31**, 911 (1999).
[19] F. Otàlora and J. M. Garcìa-Ruiz, ''Crystal growth studies in microgravity with the APCF: Computer simulation and transport dynamics,'' J. Cryst. Growth **182**, 141 (1997).
[20] F. Otàlora, M. L. Novella, J. A. Gavira, B. R. Thomas, and J. M. Garcìa-Ruiz, ''Experimental evidence for the stability of the depletion zone around a growing protein crystal under microgravity,'' Acta Crystallogr., Sect. D: Biol. Crystallogr. **57**, 412 (2001).